EPR and ENDOR Studies of Cryoreduced Compounds II of Peroxidases and Myoglobin. Proton-Coupled Electron Transfer and Protonation Status of Ferryl Hemes[†]

Roman Davydov,[‡] Robert L. Osborne,[§] Sun Hee Kim,[‡] John H. Dawson,*[,§] and Brian M. Hoffman*[,‡]

Department of Chemistry, Northwestern University, 2145 Sheridan Road, Tech K148, Evanston, Illinois 60208-3113, and Department of Chemistry & Biochemistry, University of South Carolina, 631 Sumter Street, Columbia, South Carolina 29208

Received December 21, 2007; Revised Manuscript Received March 11, 2008

ABSTRACT: The nature of the [Fe(IV)−O] center in hemoprotein Compounds II has recently received considerable attention, as several experimental and theoretical investigations have suggested that this group is not necessarily the traditionally assumed ferryl ion, $[Fe(IV)=O]^{2+}$, but can be the protonated ferryl, $[Fe(IV)-OH]^{3+}$. We show here that cryoreduction of the EPR-silent Compound II by γ-irradiation at 77 K produces Fe(III) species retaining the structure of the precursor $[Fe(IV)=O]^{2+}$ or $[Fe(IV)-OH]^{3+}$, and that the properties of the cryogenerated species provide a report on structural features and the protonation state of the parent Compound II when studied by EPR and ^{1}H and ^{14}N ENDOR spectroscopies. To give the broadest view of the properties of Compounds II we have carried out such measurements on cryoreduced Compounds II of HRP, Mb, DHP and CPO and on CCP Compound ES. EPR and ENDOR spectra of cryoreduced HRP II, CPO II and CCP ES are characteristic of low-spin hydroxy-Fe(III) heme species. In contrast, cryoreduced "globins", Mb II, Hb II, and DHP II, show EPR spectra having lower rhombicity. In addition the cryogenerated ferric "globin" species display strongly coupled exchangeable ^{1}H ENDOR signals, with $A_{max} \sim 20$ MHz and $a_{iso} \sim 14$ MHz, both substantially greater than for hydroxide/water ligand protons. Upon annealing at $T > 180$ K the cryoreduced globin compounds II relax to the low-spin hydroxy-ferric form with a solvent kinetic isotope effect, KIE > 6. The results presented here together with published resonance Raman and Mossbauer data suggest that the high-valent iron center of globin and HRP compounds II, as well as of CCP ES, is $[Fe(IV)=O]^{2+}$, and that its cryoreduction produces $[Fe(III)-O]^{+}$. Instead, as proposed by Green and co-workers (*1*), CPO II contains $[Fe(IV)-OH]^{3+}$ which forms $[Fe(III)-OH]^{2+}$ upon radiolysis. The $[Fe(III)-O]^{+}$ generated by cryoreduction of HRP II and CCP ES protonate at 77 K, presumably because the heme is linked to a distal-pocket hydrogen bonding/proton-delivery network through an H-bond to the "oxide" ligand. The data also indicate that Mb and HRP compounds II exist as two major conformational substates.

The high-valent heme peroxidase and catalase intermediates Compounds I and II provide a key to understanding the mechanism of these (*2*) and other heme enzymes, in particular serving as models for heme monooxygenase (cytochrome P450, NOS) intermediates that are yet to be fully characterized (*3*−*10*). The hemes of Compounds I and II have been oxidized by 2 and 1 equiv above the resting ferriheme state, respectively. In both instances the heme contains an [Fe(IV)−O] moiety. The second equivalent of Compound I normally exists as a π-cation radical localized on the porphyrin macrocycle; in the related CCP[1] "Compound ES," it exists as a tryptophanyl π-cation radical (*11*). The nature of the [Fe(IV)−O] center in Compounds I and II has recently received considerable attention, as several experimental and theoretical investigations suggest that this group is not necessarily the traditionally assumed ferryl ion, $[Fe(IV)=O]^{2+}$, but can be the protonated ferryl, $[Fe(IV)-OH]^{3+}$ (*8, 12*). The protonation status of the ferryl ion, as well as the possible presence of a distal-pocket proton delivery network linked to the oxo ligand, can play an important role in proton-coupled electron transfer during catalysis.

The Fe−O bond length should reflect the [Fe(IV)=O] protonation state, but reported bond lengths in Compounds II are controversial (*8*). Extended X-ray absorption fine-structure (EXAFS) investigations have indicated that the Fe−O bond length in Compounds II of myoglobin (Mb II) (*13*), HRP (HRP II) (*14*−*16*), and CCP ES (*17*) is 1.64−1.71 Å,i.e., close to that observed for the $[Fe(IV)=O]^{2+}$ of Compound I (*12, 13, 15, 18, 19*). However, high resolution crystal structures of Compounds II of myoglobin, HRP and catalase showed appreciably longer Fe−O bonds, 1.84−1.92 Å (*19*−*21*). Such a long Fe−O bond also was observed in a crystal structure of Compound ES in cytochrome *c*

[†] This work has been supported by the NIH (HL013531, B.M.H.) and the NSF (J.H.D.).

* Authors to whom correspondence should be addressed. B.M.H.: phone: (847) 491-3104; fax: 847-491-7713; e-mail: bmh@northwestern.edu.

[‡] Northwestern University.

[§] University of South Carolina.

[1] Abbreviations: Mb, myoglobin; Hb, hemoglobin; DHP, dehaloperoxidase; HRP, horseradish peroxidase; CPO, chloroperoxidase; CCP, cytochrome *c* peroxidase; Mb II, Hb II, DHP II, HRP II, CPO II, and CCP ES, Mb, Hb, DHP, HRP, CPO and CCP compounds II, respectively.

10.1021/bi702514d CCC: $40.75
Published on Web 04/12/2008

peroxidase (1.87 Å) (*22*), whose heme is electronically equivalent to the typical Compound II of HRP. A similar bond length (1.83 Å) has been reported in an EXAFS study of Compounds I of CPO (*16*) and the acid form of *Proteus mirabilis* catalase (*23*). Elongation of the Fe−O bond from 1.65−1.7 Å to 1.76−1.92 Å implies an Fe−O single bond and protonation of the oxo ligand (*8, 12*). It should be however noted that interpretationof Fe−O bond lengths in crystal structures of Compound II may be complicated by photoreduction Fe(IV) during data collection by the synchrotron radiation (*20, 24*).

Recently Mossbauer and resonance Raman spectroscopies have been used to identify the ferryl protonation status (*1, 23, 25*−*27*). Experimental data to date and DFT calculations suggest that the quadrupole splitting for Fe(IV) increases remarkably upon protonation of ferryl ion because the spin population is transferred from the oxo ligand to the iron d-orbitals (*23, 27, 28*). Mossbauer spectra of HRP II, Mb II, and CCP ES reveal only a species with quadrupole coupling of 1.4−1.6 mm/s characteristic of $[Fe(IV)=O]^{2+}$ (*8*). Mossbauer spectroscopy identified two Fe(IV) species in CPO II and PM catalase Compound II (PMC II), one with $\Delta E_Q \sim 1.4$ and one with ∼2.1−2.2 mm/s, assigned respectively to $[Fe(IV)=O]^{2+}$ and $[Fe(IV)-OH]^{3+}$ states. The relative population of the protonated form of PMC II increases with decreasing pH while the population of the predominant protonated CPO II form is independent of pH. Recently, Green and co-workers proposed to apply the empirical Badger's rule that relates bond distance and Fe(IV)−O stretching frequencies obtained from resonance Raman (RR) spectroscopy (*26*). This formula predicts stretching frequencies within the range 750−840 cm^{-1} for the $[Fe(IV)=O]^{2+}$ group, with short Fe−O bond distances of 1.62−1.70 Å, but 540−630 cm^{-1} for the longer $[Fe(IV)-OH]^{3+}$ bonds (*26*). Except for CPO II, all Compounds II studied, paradoxically including the protonated PMC II (*23*), exhibited an Fe−O frequency between 775 and 805 cm^{-1}, as expected for $[Fe(IV)=O]^{2+}$ (*8, 23*). However, the Fe−O stretch for CPO II is at 565 cm^{-1}. It is important to note that the $[Fe(IV)-OH]^{3+}$ stretch of CPO II has a relatively low intensity, and this probably accounts for its apparent absence of an RR spectra from the protonated form of PMC II (*23*). This low intensity clearly limits the use of RR spectroscopy for identification of the protonated ferryl form.

Given the significance of Compound II in catalysis (*16, 29*), it is important to clarify the character of the Compound II [Fe(IV)−O] moeity in a variety of enzymes. We show here that cryoreduction of the EPR-silent Compound II by γ-irradiation at 77 K produces Fe(III) species whose EPR and ENDOR properties report on structural details and the protonation state of the parent Compound II. The addition of an electron to an Fe(IV) heme center in frozen solution at 77 K produces a ferric state that retains the structure of the precursor; under these conditions, the frozen protein environment restricts conformational relaxation of the cryoreduced heme center to subtle changes in the geometry of Fe−ligand bond and prevents changes of the metal ligands. A cryoreduced heme center thus trapped in a nonequilibrium conformation reflected of the parent center relaxes to its equilibrium state upon progressive annealing at elevated temperatures; in many cases there is a correlation between the temperature at which the relaxation occurs and the scale of the structural changes accompanying this process. In light of these observations, cryoreduction of an $[Fe(IV)=O]^{2+}$ heme is expected to generate an $[Fe(III)-O]^{+}$ heme having a nonequilibrium conformation, while irradiation of an $[Fe(IV)-OH]^{3+}$ should generate a hydroxy−Fe(III) heme. The one restriction to this approach, however, is that in some cases the addition of an electron may be followed by a proton transfer even at temperatures below 77 K (oxy-hemeoxygenase, oxy-cytochrome P450, oxy-peroxidase) (*30*−*33*).

Earlier, Gasyna (*34*) and Petersen (*35*) reported that the product trapped during 77 K radiolytic reduction of ferryl Mb in frozen water−ethylene glycol solutions (pH 8−9) shows a rhombic EPR spectrum of a low-spin Fe(III) heme, but with $\mathbf{g} = [2.41, 2.11, \sim 1.94]$, different from low-spin hydroxy-met Mb, $\mathbf{g} = [2.58, 2.20, 1.85]$.The primary trapped species relaxes to the equilibrium hydroxy-met Mb form upon annealing at $T \geq 220$ K, doing so via two spectroscopically detected intermediates. They suggested that the initial species is the $[Fe(III)-O]^{+}$ intermediate produced by reduction of $[Fe(IV)=O]^{2+}$ (*35*). Recently, this approach was applied to CPO II (*1*). Cryoreduced CPO II exhibited an EPR spectrum different from that for resting aquo-Fe(III)-CPO, while its X-band ENDOR spectrum shows a proton ENDOR signal with $A_{max} \sim 13$ MHz, which is comparable with that for low-spin hydroxide metMb. Overall, these results are consistent with the suggested presence of $[Fe(IV)-OH]^{3+}$ in the parent CPO II.

To definitively apply the cryoreduction approach to Compounds II requires EPR and ^{1}H ENDOR characterization of the centers generated by cryoreduction of $[Fe(IV)=O]^{2+}$ and $[Fe(IV)-OH]^{3+}$ species for an extensive set of hemoproteins. To achieve this objective we have carried out comparative EPR, ENDOR, and annealing studies on cryoreduced DHP, Mb, HRP and CPO Compounds II and CCP Compound ES. Such experiments on this diverse group of protein further gives us the opportunity to broadly characterize the proton transfer processes that can occur within the heme pocket of proteins in frozen matrices.

MATERIALS AND METHODS

Myoglobin from horse heart (Sigma) and horseradish peroxidase C (type XII, RZ = 3.1) (Sigma) were used without further purification. KPi, Tris, glycerol, d_3-glycerol and dithionite were purchased from Aldrich-Sigma. 30% H_2O_2 was purchased from Fisher. Dehaloperoxidase from *Amphitrite ornata* was prepared as described (*36*), as were human hemogloglobin from whole blood (*37*), CPO from *Caldariomyces fumago* (*38*), and CCP (*39*). Ferryl Mb, DHP, Hb and CCP Compound ES were prepared by addition of a 2-fold excess of H_2O_2 to solutions of the ferric proteins in 50 mM buffer at 4 °C. HRP and CPO compounds II were prepared as described respectively in refs *40* and *1*. In typical experiments on γ-irradiation of frozen solutions at 77 K, 1−3 mM hemoprotein Compound II in 0.05 M Kpi buffer (pH 7) containing 16% v/v glycerol was applied if not mentioned otherwise.

γ-Irradiation of the frozen hemoprotein solutions at 77 K was performed typically for 16−20 h (dose rate of 0.15 Mrad/h, total dose ∼2−3 Mrad) using a Gammacell 220 ^{60}Co (*37*). Annealing at multiple temperatures over the range 77−270 K was performed by placing the EPR sample in

the appropriate bath (e.g., *n*-pentane or methanol cooled with liquid nitrogen) and then refreezing in liquid nitrogen. Irradiated samples maintained at 77 K showed no change by EPR over a period of months, indicating both the stability of the cryogenerated products and the absence of any interconversion at 77 K. As shown previously, γ-irradiation at 77 K yields an intense EPR signal at g 2.0 from radiolytically generated organic radicals; such signals are truncated in the reported spectra. In addition, γ-irradiation produces hydrogen atoms within the fused silica tubes, and these give a characteristic hyperfine doublet ($A(^1H) \approx 507$ G). As seen in all cases, as the annealing temperature is raised, radical recombination occurs and both the radical and H-atom signals decrease.

EPR/ENDOR Spectroscopy. X-band CW EPR spectra were recorded on a Bruker ESP 300 spectrometer equipped with an Oxford Instruments ESR 910 continuous He flow cryostat. CW 35 GHz EPR/ENDOR spectra were recorded on a modified Varian E-109 spectrometer. All CW Q-band EPR/ENDOR spectra were recorded at 2 K and in dispersion mode, under "rapid passage" conditions, which gives an absorption line shape (*41*). The EPR signals of cryogenerated Fe(III) species were quantitated using corresponding resting ferric hemoproteins as standards.

For a single orientation of a paramagnetic center, the first order ENDOR spectrum of a nucleus with $S = 1/2$ in a single paramagnetic center consists of a doublet with frequency given by (*41*)

$$\nu_{\pm} = |\nu_N \pm A/2| \quad (1)$$

Here, ν_N is the nuclear Larmor frequency, and A is the orientation dependent hyperfine coupling constant of the coupled nucleus. The doublet is centered at Larmor frequency and separated by A when $\nu_N > A/2$, as is the case for ^1H spectra presented here. For ^{14}N ($I = 1$), a single orientation gives a four-line pattern,

$$\nu_{\pm}(\pm) = |\nu_N \pm A/2 \pm 3P/2| \quad (1a)$$

in which both ν_+ and ν_- branches described by eq 1 are further split into two lines by quadropole coupling, $3P$. For heme pyrrole ^{14}N only the $\nu_+(\pm)$ branch is readily observed in spectra collected at 35 GHz. The full hyperfine and quadropole tensors of coupled nucleus can be obtained by analyzing a 2D field-frequency set of orientation selective ENDOR spectra collected across the EPR envelope, as described elsewhere (*41*).

RESULTS

DHP II. Irradiated DHP II shows a rhombic EPR spectrum with $\mathbf{g} = [2.44, 2.13, 1.97]$, which differs noticeably from that for low-spin ferric DHP at pH 10.5 (Figure 1, Table 1). In addition, ^1H ENDOR spectra of the cryogenerated species (Figure 2) show an exchangeable proton signal; residual intensity from the proton in the D_2O sample is due to incomplete deuteration. This signal has an unusually strong coupling, $A_{max} \approx 20$ MHz, approximately double the maximum hyperfine coupling for the hydroxide ligand in the low-spin ferric form of DHP (Figure 2, Table 2). The 2D field-frequency patterns of proton ENDOR spectra collected at multiple points along the EPR envelopes of the cryogenerated species and the equilibrium low-spin state of ferric DHP (Figure S2, Supporting Information) were analyzed to determine the hyperfine tensors of the exchangeable species. While the analysis for cryoreduced DHP II must be considered provisional because of difficulties caused by underlying proton signals from radicals, the pattern clearly is associated with a large isotropic coupling, $|a_{iso}| \sim 13$ MHz, while that for hydroxo-ferric DHP is only $|a_{iso}| \sim 4.3$ MHz (Table 2). Indeed, as shown by the data presented in Table 2, as a rule $|a_{iso}| < 4$ MHz for an OH^- (H_2O) proton.

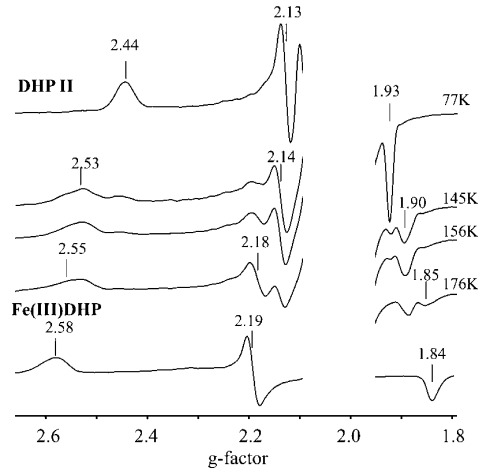

FIGURE 1: 35 GHz EPR spectra: (upper) DHP II γ-irradiated at 77 K and after annealing at 145 K, 156 K and 176 K; (lower) ferric DHP at pH 10.5. Solvent, 16% glycerol /0.05 M Kpi, pH 7.2. Conditions: 2 K; 100 kHz field modulation amplitude, 2 G; microwave frequency, 35.01 GHz (spectra are digital derivatives of absorption-display rapid passage spectra).

Table 1: EPR Parameters for Cryoreduced Compounds II and Resting Low-Spin Ferric States

hemoprotein	T_{an} (K)	g-values		
		g_1	g_2	g_3
cryoreduced CCP I		2.70	2.19	1.80
	170	2.72	2.20	1.79
ferric CCP (low-spin, pH 7)		2.72	2.20	1.79
cryoreduced HRP II (pH 6.5)				
species A		2.60	2.183	1.850
species B		2.923	2.11	1.65
cryoreduced HRP II (pH 10)				
species A		2.61	2.18	1.84
species B		2.94	2.11	1.66
ferric HRP (low-spin, pH 12)		2.97	2.11	1.64
cryoreduced CPO II		2.42	2.18	1.92
	145	2.60	2.26	1.84
ferric CPO (low-spin, pH 6.5)		2.60	2.26	1.84
cryoreduced DHP II (pH 7.0)		2.43	2.127	1.924
	145	2.53	2.14	1.90
	180	2.55	2.18	1.85
	>190	6.18	5.66	nd[a]
ferric DHP (low-spin, pH 10.5)		2.58	2.19	1.84
cryoreduced Mb II (pH >7.0)				
species A (major)		2.43	2.12	1.93
species B (minor)		2.48	2.14	~1.90
B	160	2.48	2.14	1.91
C	180	2.54	2.19	1.87
hs	>200	5.9	5.9	2.0
cryoreduced Mb II (pH 8.5)				
ls	>200	2.59	2.18	1.85
hs		5.9	5.9	2.0
met Mb (low-spin, pH 8.5)		2.59	2.18	1.85
cryoreduced Hb II (pH 7.5)		2.44	2.12	1.93
Met Hb (low-spin, pH 8.8)		2.59	2.18	1.85

[a] Not determined.

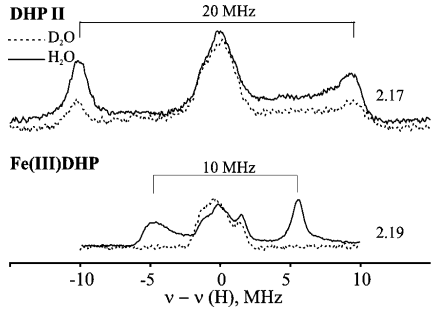

FIGURE 2: 35 GHz CW ^{1}H ENDOR spectra of cryoreduced DHP II and low-spin ferric DHP (pH 10.5) in H_2O (solid line) and D_2O (dotted line). Conditions: 2 K; modulation amplitude, 2G; rf power, 7 W; rf sweep rate, 0.5 MHz/s; rf bandwidth, 50 kHz.

Table 2: ^{1}H ENDOR Parameters for Cryoreduced Compounds II and Resting Low-Spin Ferric States

hemoprotein	A_{max} (MHz)	A_{sim} (MHz)[a]	$\|a_{iso}\|$[a]	$\|T\|$[a]	Θ (deg)
cryoreduced CCP I	11				
ferric CCP	11	−8.8, −8.8, 8.6	3	6	25
cryoreduced HRP II					
species A	12	−11, −11, 4	6	5	35
species B	10				
ferric HRP (pH > 11.5)	10				
cryoreduced CPO II	13	−13, −13, 2	8	5	35
cryoreduced DHP II	21	−20, −20, 0	13	7	45
ferric DHP (pH 10.5)	10.5	−9.4, −9.4, 5.9	4.3	5	30
cryoreduced Mb II					
species A	20	−21, −21, −1	14	7	42
species B	16				
species C	13				
met Mb (pH 8.5)	13	−11.3, −11.3, 7.1	4.5	6	35

[a] In the provisional simulations, the hyperfine tensors were constrained to be axial. The relative signs of the tensor components in a simulation are well established, but the absolute signs are not, and thus the computed isotropic and anisotropic terms, a_{iso} and T, are presented as absolute values.

The ENDOR results strongly suggest that the cryoreduced DHP II does not contain $[Fe(III)-OH]^{2+}$, which has minimal spin density on O and hence a small a_{iso} for ^{1}H. Instead, they suggest that cryoreduced DHP II contains the unprotonated $[Fe(III)-O]^+$ moiety, with a large spin density on O; the strongly coupled ^{1}H signal then must be associated with an H-bond to this O. Just such an apparently anomalous situation, weak hyperfine coupling for ^{1}H covalently bonded to an O with small spin density, but large coupling for ^{1}H H-bonded to O with large spin density, is seen in the case of H-bonded peroxo-ferric species formed by cryoreduction of $Fe(II)-O_2$ heme centers (*37, 42*). The cryogenerated $[Fe(III)-O]^+$ species relaxes upon annealing at 145 K to a form showing a slightly more anisotropic rhombic EPR spectrum, $\mathbf{g} = [2.53, 2.14, 1.9]$ (Figure 1). This intermediate still shows a strongly coupled proton ENDOR signal, $A_{max} \sim 16$ MHz, indicating that it too is an H-bonded $[Fe(III)-O]^+$ state (Figure S1, Supporting Information). Only after annealing at $T \sim 180$ K does this species convert to a state with EPR and ENDOR properties close to those for the hydroxyferric state (Table 1, Figures 1, S1); this species relaxes to the resting high-spin form at $T > 190$ K.

Mb II. The spectroscopic properties of the cryoreduced ferryl derivatives of myoglobin and hemoglobin are very similar to those of cryoreduced DHP II. However, with the "globins" we can increase the conentration of the cryogenerated species by a factor of ∼4−5 through use of more concentrated protein solutions and because the Compounds

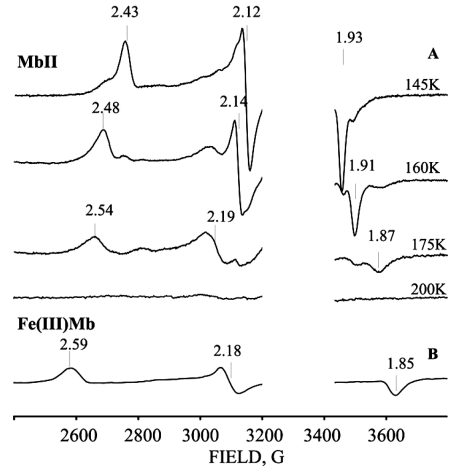

FIGURE 3: X-band EPR spectra: (**A**) cryoreduced Mb(II) (16% glycerol, 0.05 M Kpi pH 7.5) annealed at 145 K for 1 min, at 160 K for 40 min, at 175 K for 25 min and at 200 K for 1min; (**B**) Fe(III)Mb in 16% glycerol/0.05 M tris pH 8.6). Conditions: temperature, 77 K; 100 kHz field modulation amplitude, 5 G; microwave power, 10 mW; microwave frequency, 9.354.

Table 3: ^{14}N ENDOR Parameters for Cryoreduced Compounds II and Resting Low-Spin Ferric Forms of Hemoproteins at g_1

hemoprotein	species	$A(g_1)$ (MHz)	$Q(g_1)$ (MHz)
cryoreduced HRP II	A	5.76	1.17
	B	6.27	1.26
ferric HRP (pH 11.5)		6.3	1.26
		7.4	0.72
cryoreduced Mb II	A	5.37	0.9
		6.12	0.8
	C	5.69	1.14
		6.16	1.03
met Mb (pH 8.5)		5.69	1.14
		6.16	1.03

II have higher stability. Therefore, more detailed spectroscopic and kinetic studies were conducted on cryoreduced Mb II.

The EPR spectrum of the irradiated Mb II presented in Figure 3 shows two slightly different rhombic EPR signals, $\mathbf{g}(\mathbf{A}) = [2.42, 2.17, 1.93]$ (**A**, major), and $\mathbf{g}(\mathbf{B}) = [2.48, 2.14, 1.90]$ (**B**, minor), indicating the presence of two substates of the parent Compound II. Similar EPR spectra were shown by cryoreduced Hb II (Table 1). The EPR spectra of the cryogenerated species differ from these for low-spin hydroxymet Mb and Hb (Table 1). The *g*-values and relative intensities of **A** and **B** vary weakly with pH within the range pH 4.5−10, and the yield cryoreduction decreases 2−3-fold at pH < 5.The latter makes it difficult to perform spectroscopic studies on low pH samples.

During annealing at 145−160 K the **A** signal decays while the intensity of the **B** signal increases (Figure 3). For pH values below 6.5 **B** converts directly to a high-spin signal upon annealing at $T > 175$ K (not shown). Upon annealing of samples with pH > 6.5 at 175−185K **B** decays and a new intermediate, **C**, appears; its *g*-values, $\mathbf{g} = [2.54, 2.19, 1.87]$, are essentially those of low-spin met Mb (Table 1, Figure 3). For pH values within the range 6.5−8.0, further annealing above 200 K converts species **C** into an equilibrium mixture of high-spin ferric and low-spin alkaline Mb.

Like cryoreduced DHP II, the Mb II **A** form shows a strongly coupled exchangeable proton ENDOR signal, $A_{max} \sim 20$ MHz (Figure 4 upper, Table 2). Simulation of the 2D

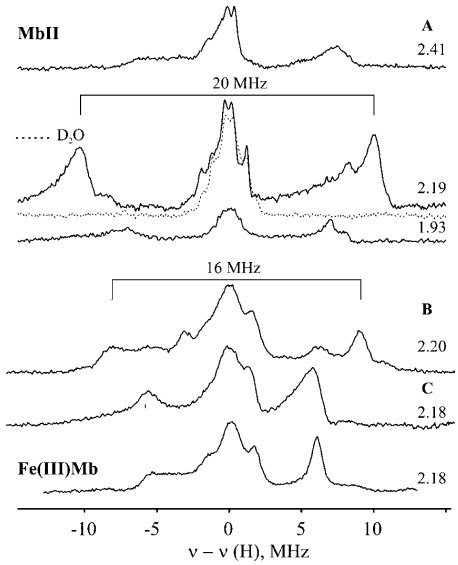

FIGURE 4: 35 GHz CW ^{1}H ENDOR spectra of cryoreduced Mb II (pH 7.5). Top, intermediate **A** at three *g*-values (dotted spectrum, with d_3-glycerol/ D_2O buffer); middle, intermediates **B** and **C** obtained during annealing of cryoreduced Mb II at 160 K and 175 K, respectively; bottom, low-spin metMb (pH 8.6). Conditions: as in Figure 2.

^{1}H ENDOR pattern of this species yields $|a_{iso}| = 14$ MHz and $T = 4.5$ MHz, values similar to those for the [Fe(III)−O]$^+$ species formed by cryoreduction of DHP II (Table 2). Pyrrole ^{14}N ENDOR spectra for this species also are different from these for low-spin hydroxy ferric Mb (Figure S3, Supporting Information). The Mb II **B** form also shows a strongly coupled exchangeable proton ENDOR signal; $A_{max} \sim 16.2$ MHz, which again is much greater than that for hydroxide ligand coordinated to ferriheme in alkaline met Mb (Figure 4, Table 2). In contrast, ^{1}H and ^{14}N ENDOR spectra for species **C** are very similar to these for low-spin hydroxy metMb (Figures 4, S3, Tables 2, 3) Overall, the *g*-values and the ^{1}H and ^{14}N ENDOR spectra (Figures 4, S3; Table 2, 3) suggest that **A** and **B** are respectively primary and relaxed [Fe(III)−O]$^+$ states that are formed upon cryoreduction of Compound II, and that in each the oxo ligand forms an H-bond to a nearby proton donor, while species **C** is a hydroxy-ferriheme state.

If this suggestion holds, then one or both of these conversions involves proton transfer and should show a significant solvent kinetic isotope effect (sKIE) (*43*). This has been tested kinetically by monitoring both conversions in H_2O/glycerol and D_2O/d_3-glycerol at pH 8, with **A** → **B** measured at 160 K and **B** → **C** at 175 K. As is common for frozen solutions, both processes are described by dispersive nonexponential kinetics, Figure 5 (*44*). The time course for the **A** → **B** conversion, as measured by the decay of **A**, is minimally effected by deuteration of the solvent, sKIE < 2. This relatively small effect (sKIE < 1.4 at ambient temperature) may be due in part to an influence of the H-bond on the conversion between **A** and **B** conformational substates. In contrast, the **B** → **C** conversion, measured by the decay of **B**, is strongly slowed, in D_2O/d_3-glycerol mixture, with sKIE ∼ 5 (Figure 5). Such an sKIE is expected at this temperature if the rate-limiting step in **B** → **C** is protonation of the oxo ligand (*45*).

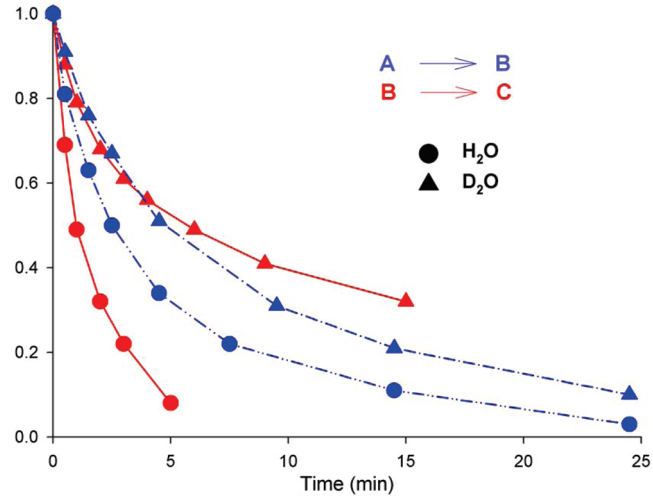

FIGURE 5: Kinetics of the conversion of the cryoreduced Mb II species **A** → **B** (decay of **A**) at 160 K (blue) and the **B** → **C** (decay of **B**) at 175 K (red). (●) H_2O, 16% glycerol/0.05 M tris pH 8.0; (▲) D_2O, 16% d_3-glycerol/0.05 M tris (pH 7.6). Intensities are scaled to value at $t = 0$.

CCP II. The spectroscopic and relaxation properties of cryoreduced Compounds II of the globin-like DHP and Mb differ markedly from these for the peroxidases. Compound ES of CCP contains a Compound II heme weakly spin-coupled to a tryptophan radical. The 77 K EPR spectrum of radiolytically reduced Compound ES shows a rhombic low-spin ferriheme EPR spectrum with **g** = [2.70, 2.19, 1.80] which differs only slightly from *g*-values for the low-spin hydroxyFe(III) resting form (Figure S4 (Supporting Information), Table 1).

The cryotrapped intermediate exhibits a 35 GHz CW ^{1}H ENDOR signal from an exchangeable proton with maximal hyperfine coupling of 12 MHz which is very similar to that for the low-spin hydroxyferri-CCP (Table 2). Likewise the two states show similar pyrrole ^{14}N ENDOR spectra (not shown). The data thus indicate that cryoreduction of CCP ES produces a low-spin hydroxy−Fe(III) complex with very similar structure to that of the equilibrium low-spin ferri-CCP. EPR, ^{1}H, and ^{14}N ENDOR spectra show that this primary product relaxes to the equilibrium form upon annealing at temperature around 170 K.

HRP II. HRP II (pH 7.5) was prepared at ambient temperature as described in Materials and Methods. Upon cryoreduction at 77 K, we observe EPR spectra from two ferriheme centers with rhombic EPR signals, **g** = [2.60, 2.18, 1.85] (species **A**) and [2.92, 2.11, 1.66] (species **B**) (Figure 6, Table 1) reflecting the existence of two different conformers in the parent HRP II. The **g**-tensor components of the more anisotropic EPR signal **B** are essentially the same as those for the alkaline form of ferric HRP at pH 12 (Figure 6, Table 1), and ^{1}H ENDOR spectra of **B** taken at g_1 show an exchangeable proton with coupling identical to that for hydroxy-Fe(III) HRP (not shown); thus we assign **B** to this state. The ratio of the **A** and **B** signals depends only weakly on pH within the range 6.5−10; in addition, at pH 10 the rhombicity of both signals slightly increases, presumably reflecting a response of the hydroxy-ferriheme to changes of heme-pocket environment with pH (Table 1).

^{1}H ENDOR was used to assign species **A**. Although the EPR spectrum of **A** is overlapped at all fields by that of the

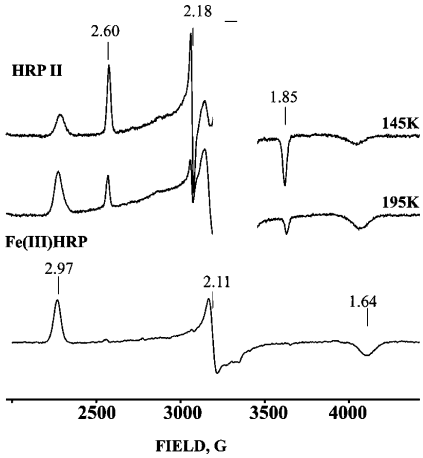

FIGURE 6: X-band EPR spectra of cryoreduced HRP II (pH 7.0) annealed at 145 K and 195 K for 1 min and Fe(III)HRP (pH 12). Conditions: $T = 12$ K; modulation amplitude, 10 G; microwave power, 2 mW; microwave frequency, 9.372.

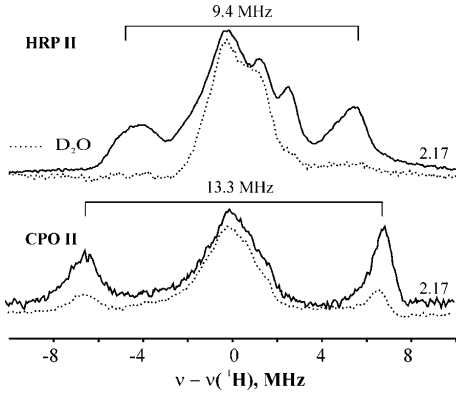

FIGURE 7: 35 GHz CW ^{1}H ENDOR spectra. (Upper) Cryogenerated HRP II species **A** in H_2O (solid line) and in D_2O (dotted line). (Lower) Likewise for cryoreduced CPO II taken at $g = 2.17$. Conditions as in Figure 2.

more rhombic signal of **B**, spectra taken outside the area of overlap show that where the two overlap the ENDOR response is dominated by that of **A**. As shown in Figure 7, ^{1}H signals from this species in H_2O have a maximal hyperfine coupling from an exchange proton with, $A_{max} \sim 12$ MHz. A 2D field-frequency pattern (not shown) can be well simulated with an axial hyperfine interaction with $|a_{iso}| = 6$ MHz (Table 2), characteristic of protons of a hydroxide/water ligand coordinated to a Fe(III) heme (*46, 47*). We therefore assign **A** as a hydroxyferric form that is trapped in a nonequilibrium structure. In agreement with this idea, during progressive annealing at higher temperatures species **A** relaxes to species **B** within the range 145−195 K (Figure 6). As a reflection of the conformational differences between **A** and **B**, ^{14}N ENDOR spectra of pyrrole nitrogens taken at g_{min} for species **A** and **B** yield noticeably different hyperfine and quadrupole couplings (Figure S5 (Supporting Information), Table 3). With continued step-annealing to temperatures above 210 K species **B** relaxes to the equilibrium, high-spin state at pH 7. Overall, these results show that HRP II exists in two conformers and that both yield an $[Fe(III)-OH]^{2+}$ state as the primary product of 77 K cryoreduction.

Cryoreduced HRP II also was generated by a two-stage cryoreduction process. HRP I formed at ambient was cryoreduced to HRP II, which was then annealed at temperatures at 220 K; this "cryogenerated-HRP II" was again

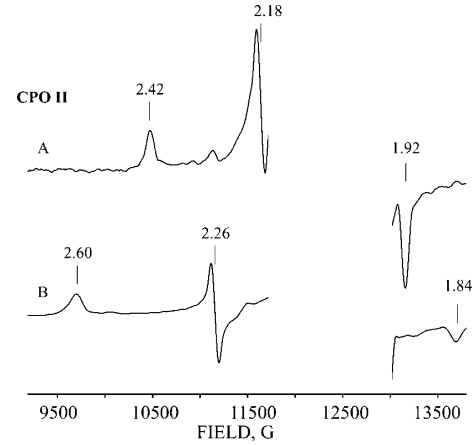

FIGURE 8: 35 GHz EPR spectra (A) of the cryoreduced CPO II and (B) after annealing at 145 K for 1 min. Conditions as in Figure 1 except for MW power, 0.06 mW, and MW frequency, 35.365.

irradiated at 77 K. The EPR spectrum of the resulting ferriheme species showed only the **B** signal. This observation indicates that when Compound II is generated at low temperatures the **B** conformer is dominant, unlike the equilibrium distribution of conformers **A** and **B** when Compound II is prepared in solution and frozen.

CPO II. Cryoreduced CPO II shows a rhombic EPR signal with g = [2.42, 2.18, 1.92], markedly different from that of the resting state (Figure 8, Table 1). The breadth of the ^{1}H ENDOR spectra of cryoreduced CPO II is set by an exchangeable proton signal; it has $A_{max} \sim 13$ MHz (Figure 7), and its 2D frequency-field pattern can be well simulated by an axial hyperfine tensor (Figure 7) with $|a_{iso}| = 4.6$ MHz, similar to the values for the hydroxide ligand in hydroxyferric Mb, HRP and CCP (Table 2). This implies that the cryoreduced state contains $[Fe(III)-OH]^{2+}$, consistent with the report by Green and co-workers which indicated that CPO II contains $[Fe(IV)-OH]^{3+}$ (*1*). Cryoreduced CPO II relaxes to the equilibrium aquo-ferric state after annealing at 145 K for 1 min.

DISCUSSION

The data presented here provides information about structural features of peroxidases and myoglobin compounds II and specifically about the protonation status of the ferryl ion. It shows unambiguously that cryoreduction of Mb II and globin-like DHP II yields $[Fe(III)-O]^+$ hemes, and thus the parent Compounds II must contain the unprotonated ferryl ion, $[Fe(IV)=O]^{2+}$. In contrast, cryoreduction of Compounds II of CPO and HRP and Compound ES of CCP at 77 K yields an $[Fe(III)-OH]^{2+}$ heme. Such a state could arise directly by cryoreduction of a $[Fe(IV)-OH]^{3+}$ precursor, or from reduction of $[Fe(IV)=O]^{2+}$ followed by proton transfer at 77 K. To gain further insight into the properties of the Compounds II and their cryoreduction products we discuss each protein separately.

Mb II and DHP II. The presence for cryoreduced Mb II and DHP II of a strongly coupled, exchangeable proton ENDOR signal, $|a_{iso}| = 13-14$ MHz (Table 2), $A_{max} \sim 20$ MHz, as well as the low rhombicities of their EPR signals, is consistent with DFT computations of the electronic structure of the $[Fe(III)-O]^+$ unit (*28*). In particular, the calculated high-spin density on oxygen (*28*) is consistent with

our assignment of the strongly coupled proton to an H-bond with the oxo ligand. Conversion of $[Fe(III)-O]^+$ to $[Fe(III)-OH]^{2+}$ through formation of the O−H convalent bond causes a major transfer of spin density from O to Fe (*28*), which in turn increases the rhombicity of the EPR signal and lessens the coupling to the hydroxide ligand proton. This correlates with the spectroscopic changes observed upon protonation of cryogenerated peroxo ferric globins (*37, 48*−*50*), which also were supported by DFT calculations (*28*). The observation that cryoreduction generates two forms of the $[Fe(III)-O]^+$ center, **A** (majority) and **B** (minority), implies that the parent Mb II exhibits two conformational substates.

The conclusion that the product of 77 K cryoreduction of Mb II is an $[Fe(III)-O]^+$ center is corroborated by the strong solvent KIE associated with its conversion to hydroxy-metMb at 180 K, which shows that this conversion indeed involves proton transfer to $[Fe(III)-O]^+$, generating $[Fe(III)-OH]^{2+}$. The latter is formed in a nonequilibrium conformation with *g*-values that differ somewhat from the resting hydroxymet-Mb; conversion to the equilibrium form occurs at ∼200 K. Observations over a range of pH indicate that Mb II contains the unprotonated $[Fe(IV)=O]^{2+}$ down to pH 4.5. DHP is a close structural analogue to the globins, and thus it is not surprising that the properties of the cryoreduced DHP II resemble those of Mb II (*36, 51*).

This conclusion is in agreement with Mossbauer, RR and EXAFS measurements (*8, 13*), but the observation of a long Fe−O bond in a crystal structure of Mb II led to the opposing conclusion that the ferryl group is protonated (*12, 52*). Our results and those of the other spectroscopies suggest that the long Fe−O bond seen in the crystal structure of Mb II reflects cryoreduction of $[Fe(IV)=O]^{2+}$ in the X-ray beam during data collection and subsequent protonation, and that the structure thus is associated with $[Fe(III)-OH]^{2+}$ (*20*).

The decoupling of the reduction and proton-transfer steps during cryoreduction of the $[Fe(IV)=O]^{2+}$ in Mb II and DHP II is precisely parallel to that seen in the cryoreduction of oxy-Mb, Hb, and isolated Hb chains (*42, 48*). Cryoreduction of the formally $[Fe(III)O_2^-]$ center in these proteins generates the $[Fe(III)(O_2^{2-})]^-$, peroxoferriheme center. It has an EPR spectrum with low rhombicity and an ENDOR signal from a strongly coupled exchangeable proton ($|a_{iso}|$ of 13−14 MHz, $A_{max} \sim 20$ MHz) associated with an H-bond to the peroxo ligand. During relaxation at ∼180 K the peroxo ligand is protonated to form a hydroperoxo ligand in a process that also proceeds with a high solvent KIE (∼5 at 180 K) (*30*). The protonation shifts spin density from O_2 to Fe and strongly lowers the hyperfine coupling, to $|a_{iso}| = 4$ MHz, and $A_{max} \approx 10-12$ MHz and increases rhombicity of the EPR signal (*37, 48, 50*). This interpretation was subsequently supported by DFT computations (*28*). The H-bonding proton was assigned to the histidine $N^{\epsilon}H$ hydrogen; the same assignment can be applied to the proton that H-bonds to $[Fe(III)-O]^+$.

CPO Compound II. The EPR spectrum of cryoreduced CPO II exhibits only one low-spin signal, with *g*-values different from these of the resting state (Table 1). We are not able to compare properties of cryoreduced CPO II with the alkaline form of ferric CPO because the latter is unstable. However, cryoreduced CPO II shows an exchangeable proton ENDOR signal with values close to those for the OH^- ligand of hydroxyferric Mb, HRP, DHP and CCP, $|a_{iso}| = 3-6$ MHz (Table 2). This observation shows that the 77 K cryoreduction product is $[Fe(III)-OH]^{3+}$. It does not prove that CPO II contains $[Fe(IV)-OH]^{3+}$, for the $[Fe(III)-OH]^+$ could form by reduction of $[Fe(IV=O)]^{2+}$ followed by protonation at 77 K. However, it is in agreement with spectroscopic and structural data of Green and coauthors (*1, 8*) which do establish that the major form of CPO II contains $[Fe(IV)-OH]^{3+}$.

Most interestingly, the hydroxide ligand of the 77 K cryogenerated $[Fe(III)-OH]^{2+}$ species in CPO is further protonated at 145 K to form the low-spin final aquoferric state. In contrast, the $[Fe(III)-OH]^+$ state generated by annealing cryoreduced Mb II at 180 K (neutral pH) converts to the stable aquoferric form by proton transfer to the hydroxide ligand only at temperatures above 200 K. These contrasting behaviors highlight the presence in CPO of an efficient distal-pocket proton delivery network that is absent in the "globins", whose heme pocket does not support low-temperature proton delivery.

Mossbauer spectroscopy indicated that CPO II also contains a minority (∼30%) of the $[Fe(IV)=O]^{2+}$ form (*27*), but only a single EPR signal is seen upon cryoreduction and only a single species was seen in the RR studies (*1*). Possible explanations include the following: (i) the minority species has a low cryoreduction yield; (ii) cryoreduction of the minority ferryl form is followed by protonation at 77 K, resulting in the same observed state for majority and minority species and (iii) lack of the minority species in the samples under the study.

HRP II and CCP ES. The ^1H ENDOR and EPR data for irradiated CCP ES and HRP II also show that cryoreduced CCP ES contains $[Fe(III)-OH]^{2+}$, and the same is true for both **A** and **B** species formed by cryoreduction of HRP II. As with Mb II, cryoreduced HRP II displays two spectroscopically distinct $[Fe(III)-OH]^{2+}$ species, **A** and **B** (Table 1), suggesting the presence of two conformational substates in HRP II whose structural differences involve the ferryl center; likewise cryoreduction also showed the presence of two conformers of oxy-HRP (*32, 33*). The relative populations of these substates depend only slightly on pH within the range pH 6−10.5 (Table 1) although the EPR properties of the species do depend on pH (Table 1) This behavior correlates with the RR report of a conversion between two forms of HRP II ($pK = 8.9$) which was attributed to an increase in the strength of the hydrogen bond to the ferryl oxygen, such as might occur upon protonation of distal His 42 (*3*). It is not clear why the RR spectra do not detect two species **A** and **B** at pH values below the p*K* of the transition.

Unlike the case of CPO II, RR, Mossbauer and EXAFS studies for CCP ES and HRP II indicate that the parent states contains $[Fe(IV)=O]^{2+}$, not $[Fe(IV)-OH]^{3+}$ (*8*). In opposition to this, long Fe−O bond distances, characteristic of a single bond, were seen in the X-ray structures of CCP ES (1.87 Å) (*22*) and HRP II (1.83 Å) (*19*). However, as noted above, it has become clear that reduction of high-valent hemes in the X-ray beam during data collection is a common occurrence (*24*), and we thus accept the spectroscopic assignments. As a result, our observations imply that the $[Fe(III)-OH]^{2+}$ hemes observed subsequent to 77 K cryoreduction are formed by reduction of the $[Fe(IV)=O]^{2+}$ to $[Fe(III)-O]^+$, followed by protonation of this unit at 77 K. This is consistent with our earlier demonstration that facile

proton transfer can occur in the heme pocket of O_2-activating enzymes down to liquid helium temperatures. Thus, proton transfer to cryogenerated peroxoferric heme center was observed at ~6−7 K in cryoreduced oxy-heme oxygenase (*30*), and at $T < 77$ K for cryoreduced oxy-P450cam (*31*), oxy-HRP (*32, 33*) and oxy-CCP (unpublished). The D251N mutation of P450cam, which was suggested (*53*) to hinder proton transfer to the heme center, and this mutation blocks the proton transfer until 160 K (*31*).

Overall, we thus see a strong correlation between the ease of proton delivery to the $[Fe(II)-O]^{2+}$ and $[Fe(III)(O_2)^{2-}]^{-}$ centers formed, correspondingly, by cryoreduction of $[Fe(IV)=O]^{2+}$ and $[Fe(III)(O_2)^{2-}]$ hemoprotein centers. In both cases protonation only occurs at 77 K or below for a peroxidase or monooxygenase enzyme, and not for a "globin". We attribute this difference to the presence of an elaborate distal-pocket hydrogen-bonding/proton-delivery network in the enzyme, connected by H-bonds to the oxy-ferroheme or ferrylheme.

ACKNOWLEDGMENT

We thank Prof. H. Halpern (University of Chicago) for access to the Gammacell 200 Irradiator.

SUPPORTING INFORMATION AVAILABLE

Five figures, two with EPR spectra, two with ^{1}H ENDOR spectra, and one with ^{14}N ENDOR spectra. This material is available free of charge via the Internet at http://pubs.acs.org.

REFERENCES

1. Stone, K. L., Behan, R. K., and Green, M. T. (2006) Resonance Raman spectroscopy of chloroperoxidase compound II provides direct evidence for the existence of an iron (IV)- hydroxide. *Proc. Natl. Acad. Sci. U.S.A. 103*, 12307–12310.
2. Dunford, H. B. (1999) *Heme peroxidases*, John Wiley, New York.
3. Terner, J., Palaniappan, V., Gold, A., Weiss, R., Fitzgerald, M. M., Sullivan, A. M., and Hosten, C. M. (2006) Resonance Raman spectroscopy of oxoiron (IV) porphyrin p-cation radical and oxoiron (IV) hemes in peroxidase intermediates. *J. Inorg. Biochem. 100*, 480–501.
4. Sono, M., Roach, M. P., Coulter, E. D., and Dawson, J. H. (1996) Heme-Containing Oxygenases. *Chem. Rev. 96*, 2841–2887.
5. Poulos, T. L., and Kraut, J. (1980) The Stereochemistry of Peroxidase Catalysis. *J. Biol. Chem. 255*, 8199–8205.
6. Poulos, T. L. (2005) Intermediates in P 450 catalysis. *Philos. Trans. R. Soc. London, Ser. A: Math., Phys. Eng. Sci. 363*, 793–806.
7. Price, J. C., Barr, E. W., Tirupati, B., Bollinger, J. M., Jr., and Krebs, C. (2003) The first direct characterization of a high-valent iron intermediate in the reaction of an a-ketoglutarate-dependent dioxygenase: A high-spin Fe(IV) complex in taurine/a-ketoglutarate dioxygenase (TauD) from Escherichia coli. *Biochemistry 42*, 7497–7508.
8. Behan, R. K., and Green, M. T. (2006) On the status of ferryl protonation. *J. Inorg. Biochem. 100*, 448–459.
9. Bollinger, J. M., and Krebs, C. (2006) Stalking intermediates in oxygen activation by iron enzymes: Motivation and method. *J. Inorg. Biochem. 100*, 586–605.
10. Makris, T. M., von Koenig, K., Schlichting, I., and Sligar, S. G. (2006) The status of high-valent metal oxo complexes in the P450 cytochromes. *J. Inorg. Biochem. 100*, 507–518.
11. Huyett, J. E., Doan, P. E., Gurbiel, R., Houseman, A. L. P., Sivaraja, M., Goodin, D. B., and Hoffman, B. M. (1995) Compound ES of Cytochrome *c* Peroxidase Contains a Trp π-Cation Radical: Characterization by CW and Pulsed Q-Band ENDOR. *J. Am. Chem. Soc. 117*, 9033–9041.
12. Hersleth, H.-P., Ryde, U., Rydberg, P., Goerbitz, C. H., and Andersson, K. K. (2006) Structures of the high-valent metal-ion haem-oxygen intermediates in peroxidases, oxygenases and catalases. *J. Inorg. Biochem. 100*, 460–476.
13. Chance, M., Powers, L., Kumar, C., and Chance, B. (1986) X-ray absorption studies of myoglobin peroxide reveal functional differences between globins and heme enzymes. *Biochemistry 25*, 1259–1265.
14. Penner-Hahn, J. E., McMurry, T. J., Renner, M., Latos-Grazynsky, L., Eble, K. S., Davis, I. M., Balch, A. L., Groves, J. T., Dawson, J. H., and Hodgson, K. O. (1983) X-ray absorption spectroscopic studies of high valent iron porphyrins. Horseradish peroxidase compounds I and II and synthetic models. *J. Biol. Chem. 258*, 12761–12764.
15. Penner-Hahn, J. E., Eble, K. S., McMurry, T. J., Renner, M., Balch, A. L., Groves, J. T., Dawson, J. H., and Hodgson, K. O. (1986) Structural Characterization of Horseradish Peroxidase Using EXAFS Spectroscopy. Evidence for Fe\dbond\O Ligation in Compounds I and II. *J. Am. Chem. Soc. 108*, 7819–7825.
16. Green, M. T., Dawson, J. H., and Gray, H. B. (2004) Oxoiron (IV) in chloroperoxidase compound II is basic: Implications for P450 chemistry. *Science 304*, 1653–1656.
17. Chance, M., Powers, L., Poulos, T., and Chance, B. (1986) Cytochrome c peroxidase compound ES is identical with horseradish peroxidase compound I in iron-ligand distances. *Biochemistry 25*, 1266–1270.
18. Jouve, H. M., Andreoletti, P., Gouet, P., Hajdu, J., and Gagnon, J. (1997) Structural analysis of compound I in hemoproteins: study on Proteus mirabilis catalase. *Biochimie 79*, 667–671.
19. Berglund, G. I., Carlsson, G. H., Smith, A. T., Szoeke, H., Henriksen, A., and Hajdu, J. (2002) The catalytic pathway of horseradish peroxidase at high resolution. *Nature (London, U.K.) 417*, 463–468.
20. Hersleth, H.-P., Uchida, T., Rohr, A. K., Teschner, T., Schuenemann, V., Kitagawa, T., Trautwein, A. X., Goerbitz, C. H., and Andersson, K. K. (2007) Crystallographic and Spectroscopic Studies of Peroxide-derived Myoglobin Compound II and Occurrence of Protonated FeIV-O. *J. Biol. Chem. 282*, 23372–23386.
21. Murshudov, G. N., Grebenko, A. I., Brannigan, J. A., Antson, A. A., Barynin, V. V., Dodson, G. G., Dauter, Z., Wilson, K. S., and Melik-Adamyan, W. R. (2002) The structures of Micrococcus lysodeikticus catalase, its ferryl intermediate (compound II) and NADPH complex. *Acta Crystallogr., Sect. D: Biol. Crystallogr. D58*, 1982–1972.
22. Bonagura, C. A., Bhaskar, B., Shimizu, H., Li, H., Sundaramoorthy, M., McRee, D. E., Goodin, D. B., and Poulos, T. L. (2003) High-resolution crystal structures and spectroscopy of native and compound I cytochrome c peroxidase. *Biochemistry 42*, 5600–5608.
23. Horner, O., Mouesca, J. M., Solari, P. L., Orio, M., Oddou, J. L., Bonville, P., and Jouve, H. M. (2007) Spectroscopic description of an unusual protonated ferryl species in the catalase from Proteus mirabilis and density functional theory calculations on related models. Consequences for the ferryl protonation state in catalase, peroxidase and chloroperoxidase. *JBIC, J. Biol. Inorg. Chem. 12*, 509–525.
24. Corbett, M. C., Latimer, M. J., Poulos, T. L., Sevrioukova, I. F., Hodgson, K. O., and Hedman, B. (2007) Photoreduction of the active site of the metalloprotein putidaredoxin by synchrotron radiation. *Acta Crystallogr., Sect. D: Biol. Crystallogr. D63*, 951–960.
25. Horner, O., Oddou, J. L., Mouesca, J. M., and Jouve, H. M. (2006) Moessbauer identification of a protonated ferryl species in catalase from Proteus mirabilis: Density functional calculations on related models. *J. Inorg. Biochem. 100*, 477–479.
26. Green, M. T. (2006) Application of Badger's Rule to Heme and Non-Heme Iron-Oxygen Bonds: An Examination of Ferryl Protonation States. *J. Am. Chem. Soc. 128*, 1902–1906.
27. Stone, K. L., Hoffart, L. M., Behan, R. K., Krebs, C., and Green, M. T. (2006) Evidence for Two Ferryl Species in Chloroperoxidase Compound II. *J. Am. Chem. Soc. 128*, 6147–6153.
28. Rydberg, P., Sigfridsson, E., and Ryde, U. (2004) On the role of the axial ligand in heme proteins: a theoretical study. *JBIC, J. Biol. Inorg. Chem. 9*, 203–223.
29. Osborne, R. L., Coggins, M. K., Walla, M., and Dawson, J. H. (2007) Horse Heart Myoglobin Catalyzes the H2O2-Dependent Oxidative Dehalogenation of Chlorophenols to DNA-Binding Radicals and Quinones. *Biochemistry 46*, 9823–9829.
30. Davydov, R., Chemerisov, S., Werst, D. E., Rajh, T., Matsui, T., Ikeda-Saito, M., and Hoffman, B. M. (2004) Proton Transfer at Helium Temperatures during Dioxygen Activation by Heme Monooxygenases. *J. Am. Chem. Soc. 126*, 15960–15961.
31. Davydov, R., Makris, T. M., Kofman, V., Werst, D. W., Sligar, S. G., and Hoffman, B. M. (2001) Hydroxylation of Camphor by

Reduced oxy-Cytochrome P450cam: Mechanistic Implications of EPR and ENDOR of Catalytic Intermediates in Native and Mutant Enzymes. *J. Am. Chem. Soc. 123*, 1403–1415.
32. Davydov, R. M., and Khangulov, S. V. (1983) ESR spectroscopy of unstable intermediates of the reduction of oxygen complexes of cytochrome P 450 and other hemoproteins. *Stud. Biophys. 95*, 97–106.
33. Denisov, I. G., Makris, T. M., and Sligar, S. G. (2002) Formation and Decay of Hydroperoxo-Ferric Heme Complex in Horseradish Peroxidase Studied by Cryoradiolysis. *J. Biol. Chem. 277*, 42706–42710.
34. Gasyna, Z. (1980) Unusual spin-state transitions in the reduction of ferrylmyoglobin at low temperature. *Biochem. Biophys. Res. Commun. 93*, 637–644.
35. Petersen, R. L., Symons, M. C. R., and Taiwo, F. A. (1989) Application of radiation and electron spin resonance spectroscopy to the study of ferryl myoglobin. *J. Chem. Soc., Faraday Trans. 1: Phys. Chem. Condens. Phases 85*, 2435–2443.
36. Osborne, R. L., Sumithran, S., Coggins, M. K., Chen, Y.-P., Lincoln, D. E., and Dawson, J. H. (2006) Spectroscopic characterization of the ferric states of Amphitrite ornata dehaloperoxidase and Notomastus lobatus chloroperoxidase: His-ligated peroxidases with globin-like proximal and distal properties. *J. Inorg. Biochem. 100*, 1100–1108.
37. Davydov, R., Kofman, V., Nocek, J., Noble, R. W., Hui, H., and Hoffman, B. M. (2004) Conformational Substates of the Oxyheme Centers in α and β Subunits of Hemoglobin as Disclosed by EPR and ENDOR Studies of Cryoreduced Protein. *Biochemistry 43*, 6330–6338.
38. Morris, D. R., and Hager, L. P. (1966) Chloroperoxidase. I. Isolation and properties of the crystalline glycoprotein. *J. Biol. Chem. 241*, 1763–1768.
39. Nocek, J. M., Leesch, V. W., Zhou, J. S., Jiang, M., and Hoffman, B. M. (2000) Multi- Domain Binding of Cytochrome *c* Peroxidase by Cytochrome c: Thermodynamic vs. Microscopic Binding Constants. *Isr. J. Chem. 40*, 35–46.
40. Chang, C. S., Yamazaki, I., Sinclair, R., Khalid, S., and Powers, L. (1993) pH dependence of the active site of horseradish peroxidase compound II. *Biochemistry 32*, 923–928.
41. Hoffman, B. M., Gurbiel, R. J., Werst, M. M., and Sivaraja, M. (1989) in *Advanced EPR. Applications in Biology and Biochemistry* (Hoff, A. J., Ed.) pp 541−591, Elsevier, Amsterdam.
42. Davydov, R., Satterlee, J. D., Fujii, H., Sauer-Masarwa, A., Busch, D. H., and Hoffman, B. M. (2003) A Superoxo-Ferrous State in a Reduced Oxy-Ferrous Hemoprotein and Model Compounds. *J. Am. Chem. Soc. 125*, 16340–16346.
43. Davydov, R., Matsui, T., Fujii, H., Ikeda-Saito, M., and Hoffman, B. M. (2003) Kinetic Isotope Effects on the Rate-Limiting Step of Heme Oxygenase Catalysis Indicate Concerted Proton Transfer/ Heme Hydroxylation. *J. Am. Chem. Soc. 125*, 16208–16209.
44. Siebrand, W., and Wildman, T. A. (1986) Dispersive kinetics: a structural approach to nonexponential processes in disordered media. *Acc. Chem. Res. 19*, 238–243.
45. Knapp, M. J., and Klinman, J. P. (2002) Environmentally coupled hydrogen tunneling: Linking catalysis to dynamics. *Eur. J. Biochem. 269*, 3113–3121.
46. LoBrutto, R., Scholes, C. P., Wagner, G. C., Gunsalus, I. C., and Debrunner, P. G. (1980) Electron Nuclear Double Resonance of Ferric Cytochrome P450CAM. *J. Am. Chem. Soc. 102*, 1167–1170.
47. Fann, Y.-C., Gerber, N. C., Osmulski, P. A., Hager, L. P., Sligar, S. G., and Hoffman, B. M. (1994) ENDOR Determination of Heme Ligation in Chloroperoxidase and Comparison with Cytochrome P-450Cam. *J. Am. Chem. Soc. 116*, 5989–5990.
48. Kappl, R., Höhn-Berlage, M., Hüttermann, J., Bartlett, N., and Symons, M. C. R. (1985) Electron spin and electron nuclear-double resonance of the [FeO2]− centre from irradiated oxyhemo- and oxymyoglobin. *Biochim. Biophys. Acta 827*, 327–343.
49. Davydov, R., Macdonald, I. D. G., Makris, T. M., Sligar, S. G., and Hoffman, B. M. (1999) EPR and ENDOR of Catalytic Intermediates in Cryoreduced Native and Mutant oxy-Cytochromes P450cam: Mutation-Induced Changes in the Proton Delivery System. *J. Am. Chem. Soc. 121*, 10654–10655.
50. Symons, M. C. R., and Petersen, R. L. (1978) Electron capture by Oxyhaemoglobin: an e.s.r. study. *Proc. R. Soc. London B 201*, 285–300.
51. Belyea, J., Gilvey, L. B., Davis, M. F., Godek, M., Sit, T. L., Lommel, S. A., and Franzen, S. (2005) Enzyme function of the globin dehaloperoxidase from amphitrite ornata Is activated by substrate binding. *Biochemistry 44*, 15637–15644.
52. Hersleth, H. P., Dalhus, B., Gorbitz, C. H., and Andersson, K. K. (2002) An iron hydroxide moiety in the 1.35 ANG. resolution structure of hydrogen peroxide derived myoglobin compound II at pH 5.2. *JBIC, J. Biol. Inorg. Chem. 7*, 299–304.
53. Vidakovic, M., Sligar, S. G., Li, H., and Poulos, T. L. (1998) Understanding the Role of the Essential Asp251 in Cytochrome P450cam Using Site-Directed Mutagenesis, Crystallography, and Kinetic Solvent Isotope Effect. *Biochemistry 37*, 9211–9219.

BI702514D